JMEPEG
https://doi.org/10.1007/s11665-019-04013-2

1059-9495/$19.00

Characterization of a Cast Duplex Stainless Steel with 3.0%Cu and Modeling of Precipitation Hardening

H.M.L.F. de Lima, S.S.M. Tavares, W.S. Araujo, J. Dille, and L. Malet

(Submitted October 21, 2018; in revised form February 4, 2019)

Duplex stainless steels (DSSs) are corrosion-resistant alloys extensively used in aggressive environments. Cast DSSs may be selected for pipes, valves and pumps in chemical, petrochemical and nuclear industries. The grade steel ASTM A890 1B is an example of cast DSS with 2.7-3.3%Cu addition. Copper increases the resistance to many types of corrosion, especially in non-oxidizing environments. When the copper content is higher than 2%, the steel can be precipitation-hardened. In this work, the precipitation hardening of a DSS ASTM A890 1B steel with 3.0%Cu was studied and modeled for aging temperatures in the 450-600 °C range. Copper precipitates in the ferrite phase, but remains in solid solution in the austenite. The age hardening curves were modeled by $\Delta H = K(t)^n$ model, where ΔH is the increase in hardness, t is the aging time, and K and n are constants to be determined. The microstructure and substructure were investigated by scanning electron and transmission electron microscopes.

Keywords aging, precipitation hardening, stainless steel

1. Introduction

Duplex stainless steels (DSSs) and superduplex stainless steels (SDSSs) are corrosion-resistant alloys (CRAs) with a biphasic microstructure of ferrite (δ) and austenite (γ). This family of stainless steels combines high strength, toughness, ductility, and high resistance to different types of corrosions. For many applications, the best combination of properties is obtained with equal parts of ferrite and austenite and absence of other phases (Ref 1, 2). However, some alloys may be precipitation-hardened to improve mechanical and wear resistance. Two types of precipitation reactions may be used in DSS: the ferrite decomposition by $\delta \rightarrow \alpha' + \alpha''$ (Ref 3, 4) and the Cu-rich particles precipitation studied in this work.

DSSs components may be produced by different fabrication processes, including forging, rolling, welding, casting and powder metallurgy. Cast DSSs are used in cooling water pipes, valve bodies, pump casings and elbows of chemical, petrochemical and nuclear industries (Ref 5-7). Solution treatment is frequently performed in DSSs and SDSSs to adjust the ferrite and austenite contents and improve mechanical and corrosion resistance properties (Ref 8, 9). In the case of DSSs, the solution treatment is carried out at 1040 °C minimum (Ref 10), followed by water cooling.

H.M.L.F. de Lima and **W.S. Araujo**, Departamento de Engenharia Metalúrgica e Materiais, Universidade Federal do Ceará, Av. Mister Hull, s/n - Pici, Fortaleza, CE, Brazil; **S.S.M. Tavares**, Departamento de Engenharia Mecânica, Universidade Federal Fluminense, Rua Passo da Pátria, 156, Niterói, RJ CEP 24210-240, Brazil; and **J. Dille** and **L. Malet**, 4MAT, Materials Engineering, Characterization, Processing and Recycling, Université Libre de Bruxelles, 50 Avenue FD Roosevelt, CP194/03, Brussels, Belgium. Contact e-mail: ssmtavares@terra.com.br.

Some commercial stainless steels may contain copper addition to improve corrosion resistance in non-oxidizing environments (Ref 2, 11-14). UNS S32760 is an example of SDSS grade with 0.5-1.0%Cu addition to improve resistance to HCl solutions. The wrought grade UNS S32550 contains at least 1.5%Cu to obtain optimum corrosion resistance in 70%H_2SO_4 hot solution (Ref 2). Higher copper additions ($\geq$ 2%), such as found in cast UNS grades J93370 and J93372, can promote age hardening due to the precipitation of extra fine Cu-rich particles upon aging in the 300-600 °C range (Ref 2). This strengthening mechanism is especially interesting for cast components which cannot be thermomechanically treated to improve strength and wear resistance. Besides this, aged DSS with 3.0%Cu addition was more resistant to pitting corrosion due to *Pseudomonas aeruginosa* biofilm (Ref 13).

In this work, the age hardening of a cast DSS with 3.0%Cu was studied. The main objectives were to model the aging hardening curves and determine the activation energy for precipitation.

2. Experimental

The DSS used in this work corresponds to cast bars with 10 mm thickness of UNS J93372 (ASTM A890 grade 1B (Ref 10)). The chemical composition of the material presented in Table 1 was determined by combustion method (C, S and N) and by inductively coupled plasma spectroscopy optical emission spectroscopy (ICP OES) (other elements). The pitting resistance equivalent number (PREN) calculated by PREN = (%Cr) + 3.3(%Mo) + 16(%N) is also reported in Table 1.

The microstructure was characterized by optical microscope (OM) and scanning electron microscope (SEM) with energy-dispersive x-ray spectroscopy (EDS). Specimens for OM were polished and etched with Behara's solution (80 mL distilled water, 20 mL HCl and $K_2S_2O_5$).

The TEM investigations were performed using a Philips CM20 transmission electron microscope operating at 200 kV. The thin foils were prepared by twin-jet electropolishing in a

Published online: 08 April 2019

chemical solution of 10% perchloric acid and 90% ethanol at 20.5 V and 15 °C.

Specimens of the cast bars were solution-treated at 1100 °C for 40 min and water-quenched. Then, cylinders with ~ 8 mm diameter and 10 mm thickness were cut from the bar. These cylinders were aged at 450, 475, 500, 550 and 600 °C for different periods of time.

Vickers hardness with 10 kgf load of each specimen was measured. Some selected specimens were also tested with microhardness with load 25 gf. In these specimens, the microhardness of ferrite and austenite was measured.

3. Results and Discussion

Figure 1(a) presents the microstructure of the solution-treated specimen, containing 55 ± 5% of ferrite. Specimens aged at 450, 550 and 600 °C, for 1 h, are shown in Fig. 1(b), (c) and (d), respectively. The austenite volume fraction (AVF) was measured by image analysis of 10 fields, and the result are presented in Table 2. As expected, the AVF slightly increased with aging treatments, i.e., small amounts of secondary austenite (γ_2) precipitated during treatments in the 450-600 °C range.

An important microstructural characteristic of the cast DSS is the presence of nonmetallic inclusions, with round shape, as shown in Fig. 2. The EDS composition maps of one of these inclusions reveals the presence of O, Al, Si, Mn and S (Fig. 3). These results reveal a complex inclusion with an aluminum-manganese-silicate ($(Al,Mn,Si)_xO_y$) and some (Mn,Mo)S sulfides precipitated over it. These types of inclusions are very stable and do not dissolve in the solution heat treatment.

Other valuable information from SEM/EDS is the partition of elements between ferrite and austenite. Table 3 shows the average results from the analysis of three points in ferrite and three points in austenite. It is observed a general rule: austenitizing elements, such as Ni, Cu and Mn, are more

Table 1 Chemical composition of DSS ASTM A890 grade 1B (UNS J93372) (wt.%)

C	Cr	Ni	Mn	Si	Mo	Cu	N	Fe	PREN
0.043	25.64	4.51	0.68	0.80	2.01	3.01	0.21	Bal.	35.6

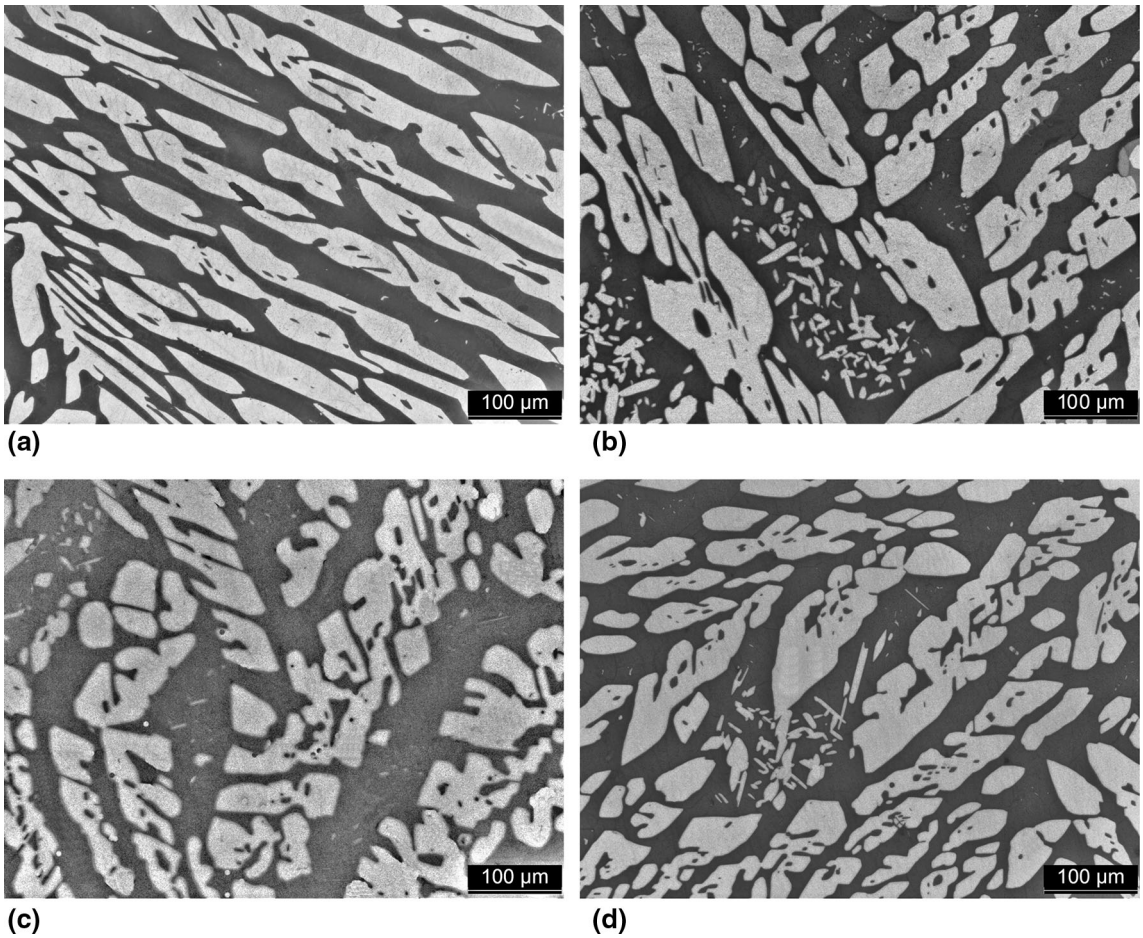

Fig. 1 Microstructures of specimens (a) solution treated; (b) aged at 450 °C/1 h; (c) aged at 550 °C/1 h; and (d) aged at 600 °C/1 h

concentrated in austenite, and ferritizing elements, such as Cr, Mo and Si, are more concentrated in ferrite. Nitrogen cannot be analyzed by EDS, but published data predict the strong concentration of this element in the austenite, with partition coefficients (k) varying from 0.1 to 0.2, depending on the alloy and temperature (Ref 2).

Figure 4 shows hardness data as a function of aging time. The individual hardening curves may be modeled by Eq 1 (Ref 15, 16):1

$$\Delta H = K(t)^n, \quad \text{(Eq 1)}$$

Table 2 Austenite volume fractions measured in specimens unaged and aged for 1 h

Unaged	450 °C/1 h	500 °C/1 h	550 °C/1 h	600 °C/1 h
45.5 ± 2.0	48.0 ± 1.5	49.0 ± 1.1	46.8 ± 2.5	48.1 ± 1.4

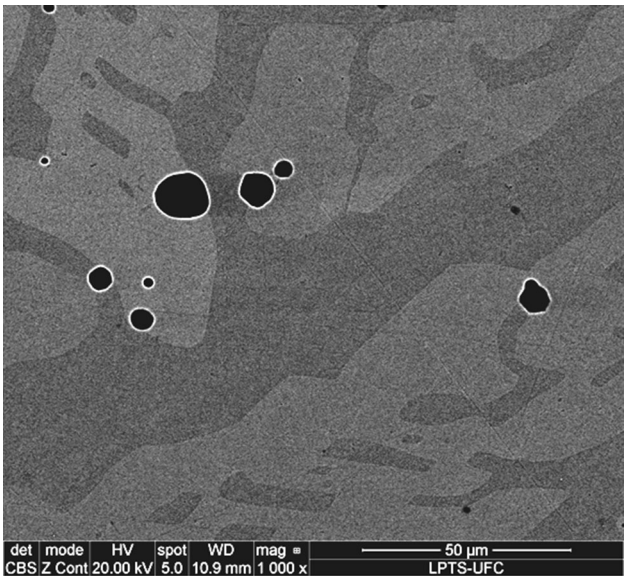

Fig. 2 Backscattered electrons image of specimen aged at 500 °C for 1 h showing austenite, ferrite and inclusions

where ΔH is the Vickers hardness variation, t is the time in minutes, and K and n are constants to be determined. This equation derives from the Johnson–Mehl–Avrami model and is applicable for the early stages of aging, i.e., does not apply to overaging (Ref 15, 16). It was used in previous works to describe the aging kinetics on maraging steels (Ref 15, 17) and Fe-12Ni-6Mn alloy (Ref 16).

Figure 5(a), (b) and (c) shows the modeled curve and experimental data for temperatures 450, 475 and 500 °C. Table 4 shows the values of K and n obtained in each temperature from the $\ln(\Delta H) \times \ln(t)$ fitting. The hardening curve of specimens aged at 550 and 600 °C could not be

Table 3 Chemical compositions estimated by EDS in ferrite and austenite phases

Phase	%Cr	%Fe	%Ni	%Mo	%Cu	%Si	%Mn
δ (ferrite)	23.9	61.9	7.3	1.7	3.4	0.9	0.8
γ (austenite)	28.3	60.6	4.6	2.7	2.4	1.1	0.7

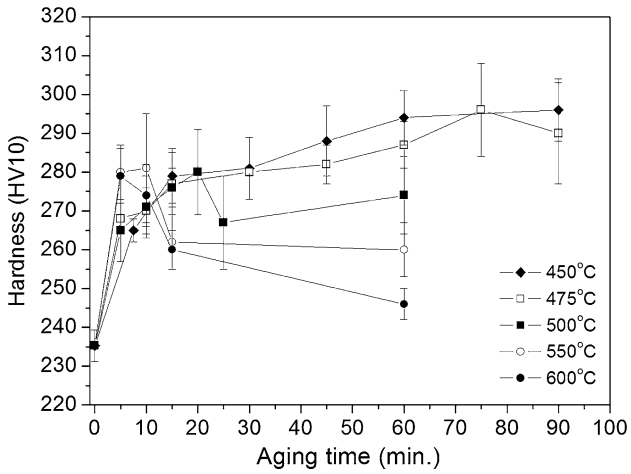

Fig. 4 Hardness × aging time for 450, 475, 500, 550 and 600 °C treatments

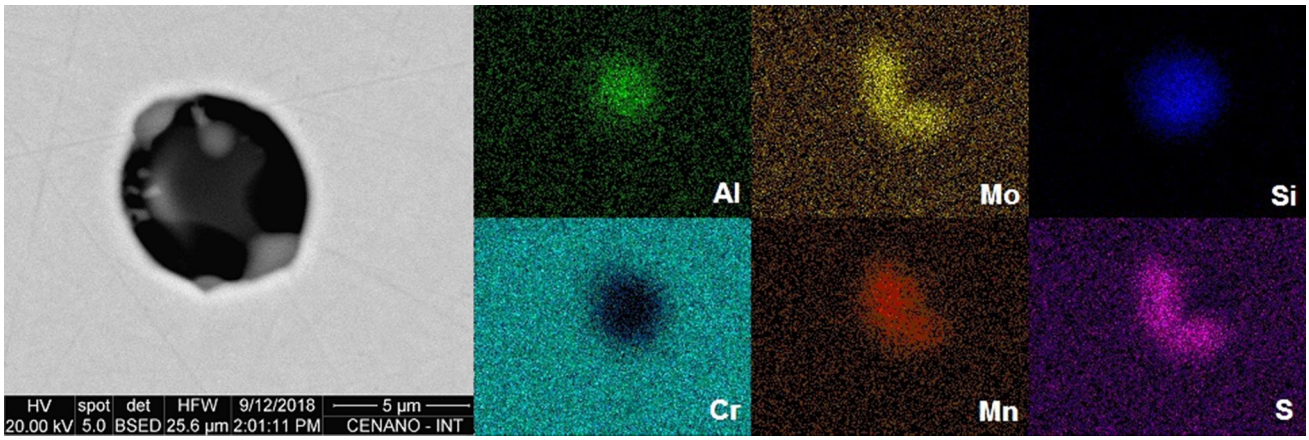

Fig. 3 EDS composition maps of inclusion

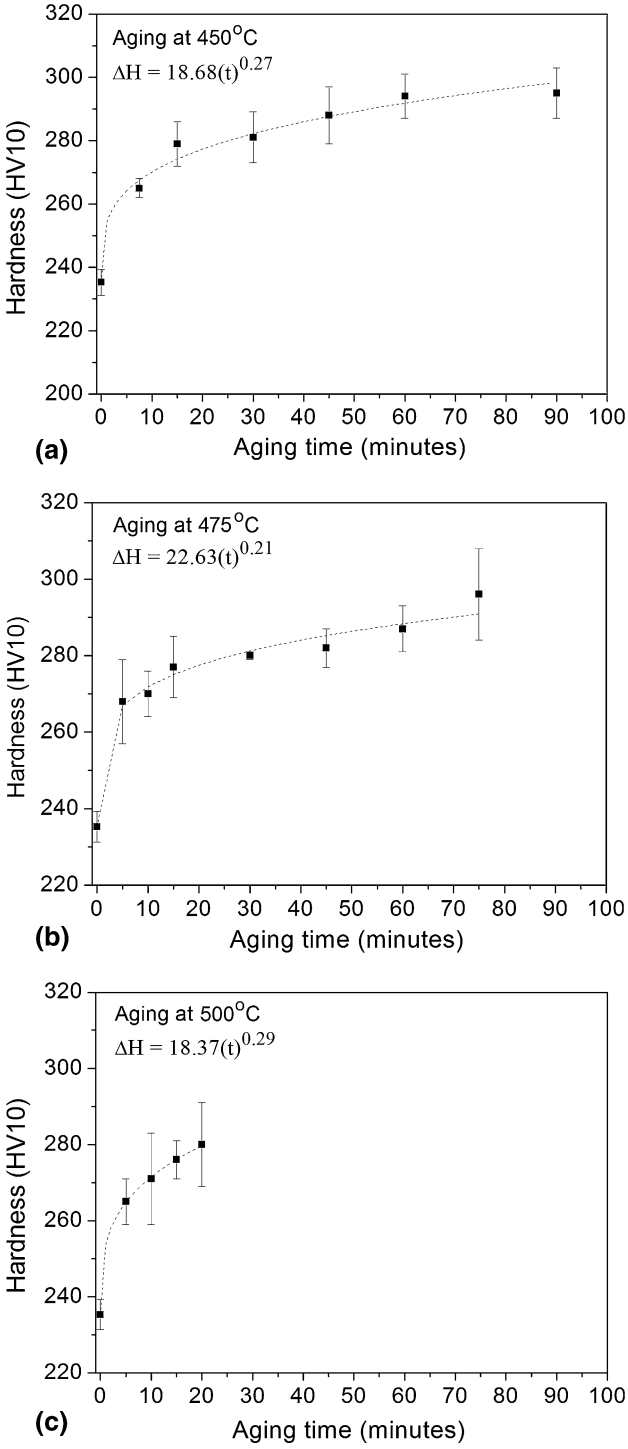

Fig. 5 Age hardening curves: (a) 450 °C; (b) 475 °C; (c) 500 °C

Table 4 Parameters *n* and *K* obtained in temperatures 450, 475 and 500 °C

Temperature, °C	*n*	*K*	R^2
450	0.27	18.7	0.924
475	0.21	22.6	0.924
500	0.29	18.4	0.997

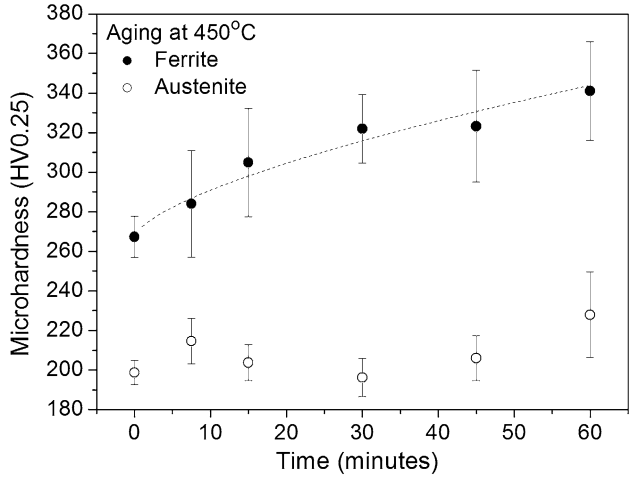

Fig. 6 Microhardness evolution in ferrite and austenite

modeled because the peak of hardness occurred with 10 and 5 min of aging, respectively.

Figure 6 shows the microhardness evolution of individual phases with aging time at 450 °C. As observed, only ferrite undergoes hardening.

TEM investigation of the specimen aged at 450 °C for 1 h reveals fine (< 10 nm) and intense precipitation in the ferrite (Fig. 7a). Coherency contrast can be observed around the precipitates. At this temperature, the ferrite phase of DSSs may also undergo the $\delta \rightarrow \alpha' + \alpha''$ reaction (Ref 3, 4), but the typical modulated aspect of the decomposed ferrite (Ref 18) was not observed by TEM, probably due to the short aging time (1 h). In opposite, the bright-field image from austenite did not reveal the presence of such fines precipitates, but only stacking faults and planar arrays of dislocations (Fig. 7b). The solubility of copper in austenite is about 4% (Ref 19, 20). Although the copper content in austenite is higher than in ferrite, 3.4% according to Table 3, copper is entirely dissolved in the FCC phase. On the other hand, the copper solubility limit in the BCC ferrite phase is about 0.2%, which is much lower than the content measured by EDS (Table 3). This can explain an intense precipitation of copper-rich particles in the ferrite as shown in Fig. 7(a). The literature indicates that the precipitation of Cu-rich particles in ferrite during aging between 450 and 600 °C is a multi-step process (Ref 21-24). A recent simulation performed by Zhou et al. (Ref 23) revealed that the precipitation sequence is: (1) Cu BCC, (2) Cu 9R and (3) Cu FCC. Moreover, this sequence was in good agreement with their experimental results. Following Han et al. (Ref 24), the lattice parameter of Cu BCC (0.295 nm) is slightly greater than the ferrite lattice parameter (0.286 nm) in a low-carbon steel. The degree of mismatch between Cu BCC and matrix is less than 5%, implying coherent relationship.

Electron diffraction permits to identify the coherent precipitates observed in Fig. 7(a) as Cu-rich BCC precipitates. Figure 7(c) shows the electron diffraction pattern of the region corresponding to Fig. 7(a). It can be indexed as the superposition of two electron diffraction patterns: diffraction pattern (*M*) of the ferrite matrix with [− 103] zone axis and diffraction pattern (*P*) of Cu-rich BCC precipitates with [100] zone axis. The precipitation of fine coherent Cu-rich BCC particles explains the hardness increase in ferrite shown in Fig. 6.

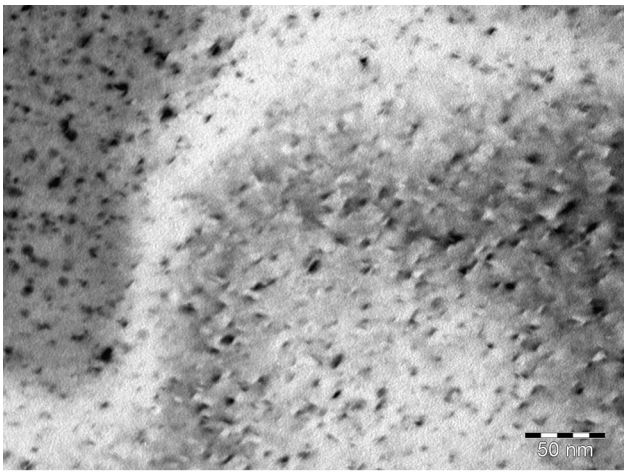

(a)

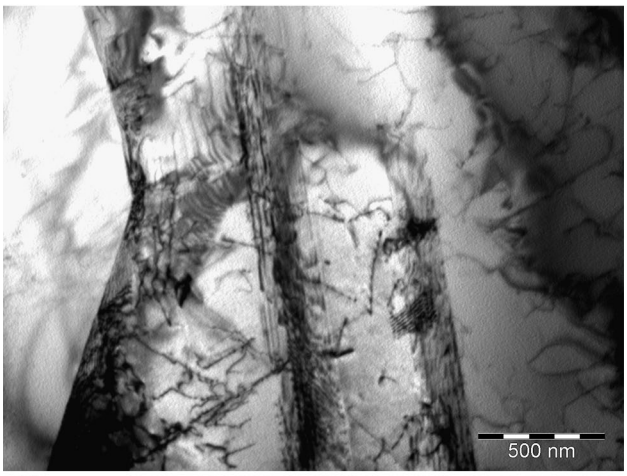

(b)

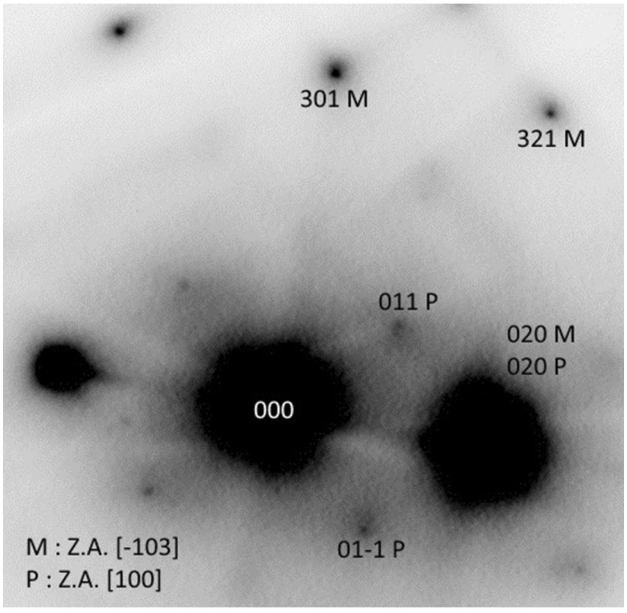

(c)

Fig. 7 (a) TEM bright-field image of ferrite with Cu-rich precipitates; (b) TEM bright-field image of austenite showing dislocations and stacking faults; (c) electron diffraction pattern of the region corresponding to (a)

Table 5 Peaks of hardness and respective aging time

	475	500	550	600
Hardness peak	296 ± 12	280 ± 11	281 ± 12	279 ± 7
Aging time	75	20	10	5

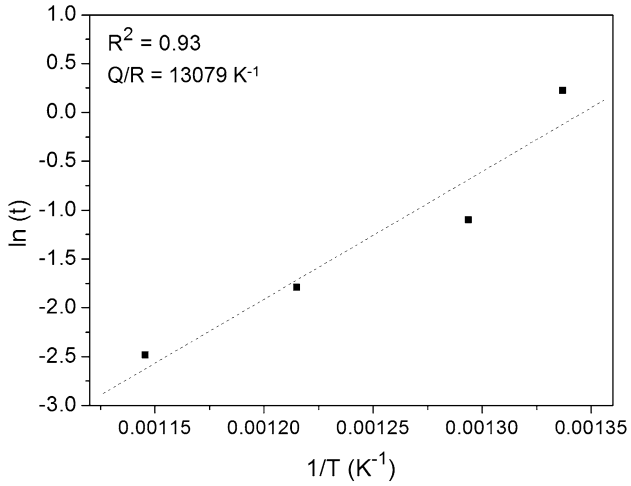

Fig. 8 Plot of $\ln(t)$ vs. $1/T$ to determine the activation energy for precipitation

Table 5 presents the peak of hardness and the corresponding aging time for each temperature. The peak was not achieved in the aging at 450 °C till 90 min.

The activation energy for copper-rich phase precipitation may be obtained from the Arrhenius Eq 2:

$$\ln(t) = Q/(RT) + \text{constant}, \quad \text{(Eq 2)}$$

where Q is the activation energy for the precipitation (kJ/mol); t the time taken to attain peak hardness at each temperature (h); R the universal gas constant (0.008314 kJ/mol K); and T the aging temperature (K). From the plot of logarithm of the time to the peak hardness against $1/T$ (Fig. 8), the activation energy was estimated as 108.7 kJ/mol. The activation energy must be strongly influenced by the chemical composition of the steel, which affects the copper diffusivity in the ferrite phase. As far as we investigated, there are no other published values of activation energy for copper-rich phase precipitation in DSSs. The activation energy encountered (108.7 kJ/mol) is of the same order of precipitation hardening of Ti- and Mo-alloyed maraging steels (Ref 17).

4. Conclusions

The microstructure, substructure and age hardening curves of a cast ASTM A890 grade 1B steel were studied. The main conclusions are:

- The material contains stable round complex inclusions of aluminum-manganese-silicate ($(Al, Mn, Si)_xO_y$), with (Mn, Mo)S sulfides precipitated over them.
- The precipitation hardening of a cast DSS ASTM A890 grade 1B can be modeled by $\Delta H = K(t)^n$ equation.

Copper concentration in austenite is higher than in ferrite. However, the precipitation of copper-rich phase occurs exclusively in the ferrite phase because the copper solubility is much lower in ferrite than in austenite.

Electron diffraction confirms the precipitation of Cu-rich BCC phase. The fine (< 10 nm) precipitates are coherent with the matrix and induces a hardening of the ferrite phase.

The activation energy for Cu-rich BCC precipitation in the DSS steel studied was 108.7 kJ/mol.

Acknowledgments

Authors are grateful to Brazilian Research Agencies CAPES, CNPq and FAPERJ for financial support.

References

1. ASM Speciality Handbook: Stainless Steels. ASM International
2. R.N. Gunn, *Duplex Stainless Steels: Microstructure, Properties and Applications*, Abington Publishing, Cambridge, 2003
3. A. Loureiro, V.C. da Costa, J.M. Pardal, T.R. Montenegro, and S.S.M. Tavares, Influence of Heat Treatments at 475 °C and 400 °C on the Pitting Corrosion Resistance and Sensitization of UNS S32750 and UNS S32760 Superduplex Stainless Steels, *Mater. Corros.*, 2012, **63**, p 522
4. S.S.M. Tavares, J.M. Pardal, H.F.G. de Abreu, C.S. Nunes, and M.R. da Silva, Tensile Properties of Duplex UNS S32205 and Lean Duplex UNS S32304 Steels and the Influence of Short Duration 475 °C Aging, *Mater. Res.*, 2012, **15**, p 859
5. Y.H. Yao, J.F. Wei, and Z.P. Wang, Effect of Long-Term Thermal Aging on the Mechanical Properties of Casting Duplex Stainless Steels, *Mater. Sci. Eng. A*, 2012, **551**, p 116
6. S. Lee, P.T. Kuo, K. Wichman, and O. Chopra, Flaw Evaluation of Thermally Aged Cast Stainless Steel in Light-Water Reactor Applications, *Int. J. Press. Vess. Pip.*, 1997, **72**, p 37
7. J. Yoganandh, S. Natarajan, and S.P. Kumaresh Babu, Erosive Wear Behavior of High-Alloy Cast Iron and Duplex Stainless Steel Under Mining Conditions, *J. Mater. Eng. Perform.*, 2015, **24**, p 3588
8. M. Martins and L.C. Casteletti, Heat Treatment Temperature Influence on ASTM 890 GR 6A Superduplex Stainless Steel Microstructure, *Mater. Charact.*, 2005, **55**, p 225
9. J.-S. Lee, S.-H. Jeon, and Y.-S. Park, Effects of Solution Annealing Temperature on the Galvanic Corrosion Behavior of the Super Duplex Stainless Steels, *J. Mater. Eng. Perform.*, 2013, **22**, p 557
10. ASTM A890—standard specification for castings, iron–chromium–nickel–molybdenum corrosion-resistant, duplex (austenitic/ferritic) for general application. ASTM, West Conshohocken; 2000
11. I.A. Armas and S. Degallaix-Moreuil, *Duplex Stainless Steels*, Wiley, New York, 2009
12. M. Seo, G. Hultquist, C. Leygraf, and N. Sato, The Influence of Minor Alloying Elements (Nb, Ti and Cu) on the Corrosion Resistivity of Ferritic Stainless Steel in Sulfuric Acid Solution, *Corros. Sci.*, 1986, **26**, p 949
13. S.H. Jeon, H.J. Kim, K.H. Kong, and Y.S. Park, Effects of Copper Addition on the Passivity and Corrosion Behavior of 27Cr-7Ni Hyper Duplex Stainless Steels in Sulfuric Acid Solution, *Mater. Trans.*, 2015, **56**, p 78
14. P. Li, Y. Zhao, Y. Liu, Y. Zhao, D. Xu, C. Yang, T. Zhang, T. Gu, and K. Yang, Effect of Cu Addition to 2205 Duplex Stainless Steel on the Resistance Against Pitting Corrosion by the *Pseudomonas aeruginosa* Biofilm, *J. Mater. Sci. Technol.*, 2017, **33**, p 23
15. W. Sha, Quantification of Age Hardening in Maraging Steels and Ni-Base Superalloys, *Scr. Mater.*, 2000, **42**, p 549
16. E.A. Wilson, Quantification of Ageing Hardening in an Fe-12Ni-6Mn, *Scr. Mater.*, 1997, **36**(10), p 1179–1185
17. J.M. Pardal, S.S.M. Tavares, V.F. Terra, M.R. da Silva, and D.R. Dos Santos, Modeling of Precipitation Hardening During the Aging and Overaging of 18Ni-Co-Mo-Ti Maraging 300 Steel, *J. Alloys Compd.*, 2005, **393**, p 109
18. Y.-C. Hsieh, L. Zhang, T.-F. Chung, Y.-T. Tsai, J.-R. Yang, T. Ohmura, and T. Suzuki, In-Situ Transmission Electron Microscopy Investigation of the Deformation Behavior of Spinodal Nanostructured δ-Ferrite in a Duplex Stainless Steel, *Scr. Mater.*, 2016, **125**, p 44
19. J. Banas and A. Mazurkiewicz, The Effect of Copper on Passivity and Corrosion Behaviour of Ferritic and Ferritic–Austenitic Stainless Steels, *Mater. Sci. Eng. A*, 2000, **277**, p 183
20. I. Le May and L.M. Schetky, *Copper in Iron and Steel*, Wiley, New York, 1982
21. H.R. Habibi Bajguirani, C. Servant, and G. Cizeron, TEM Investigation of Precipitation Phenomena Occurring in PH 15-5 Alloy, *Acta Metall. Mater.*, 1993, **41**(5), p 1613
22. Y.U. Heo, Y.K. Kim, J.S. Kim, and J.K. Kim, Phase Transformation of Cu Precipitates from bcc to fcc in Fe-3Si-2Cu Alloy, *Acta Mater.*, 2013, **61**, p 519
23. T. Zhou, R.P. Babu, J. Odqvist, H. Yu, and P. Hedström, Quantitative Electron Microscopy and Physically Based Modelling of Cu Precipitation in Precipitation-Hardening Martensitic Stainless Steel 15-5 PH, *Mater. Des.*, 2018, **143**, p 141
24. G. Han, Z.J. Xie, Z.Y. Li, B. Lei, C.J. Shang, and R.D.K. Misra, Evolution of Crystal Structure of Cu Precipitates in a Low Carbon Steel, *Mater. Des.*, 2017, **135**, p 92